REPORT DOCUMENTATION PAGE

Form Approved
OMB No. 0704-0188

1. REPORT DATE *(DD-MM-YYYY)*	2. REPORT TYPE	3. DATES COVERED *(From – To)*
23 May 2017	Journal Article	January 2014 – December 2015

4. TITLE AND SUBTITLE
Utilization of MRI for Cerebral White Matter Injury in a Hypobaric Swine Model—Validation of Technique

5a. CONTRACT NUMBER

5b. GRANT NUMBER

5c. PROGRAM ELEMENT NUMBER

6. AUTHOR(S)
Jennifer A. McGuire, AS; Col Paul M. Sherman, USAF, MC; Erica Dean, BSN;
Maj Jeremy M. Bernot, USAF, MC; Laura M. Rowland, PhD;
Col Stephen A. McGuire, USAF, MC (Ret.); Peter V. Kochunov, PhD

5d. PROJECT NUMBER

5e. TASK NUMBER

5f. WORK UNIT NUMBER

7. PERFORMING ORGANIZATION NAME(S) AND ADDRESS(ES)
USAF School of Aerospace Medicine
Aeromedical Research Dept/FHOH
2510 Fifth St., Bldg. 840
Wright-Patterson AFB, OH 45433-7913

8. PERFORMING ORGANIZATION REPORT NUMBER

AFRL-SA-WP-JA-2016-0016

9. SPONSORING / MONITORING AGENCY NAME(S) AND ADDRESS(ES)

10. SPONSORING/MONITOR'S ACRONYM(S)

11. SPONSOR/MONITOR'S REPORT NUMBER(S)

12. DISTRIBUTION / AVAILABILITY STATEMENT

DISTRIBUTION STATEMENT A. Approved for public release. Distribution is unlimited.

13. SUPPLEMENTARY NOTES
Cleared, 88PA, Case # 2016-1995, 20 Apr 2016. Mil Med. 2017; 182(5/6): e1757-e1764.

14. ABSTRACT
Background: Repetitive hypobaric exposure in humans induces subcortical white matter change, observable on magnetic resonance imaging (MRI) and associated with cognitive impairment. Similar findings occur in traumatic brain injury (TBI). We are developing a swine MRI-driven model to understand the pathophysiology and to develop treatment interventions. Methods: Five miniature pigs (*Sus scrofa domestica*) were repetitively exposed to nonhypoxic hypobaria (30,000 feet/FIO_2 100%/transcutaneous PO_2 >90%) while under general anesthesia. Three pigs served as controls. Pre-exposure and postexposure MRIs were obtained that included structural sequences, dynamic contrast perfusion, and diffusion tensor quantification. Statistical comparison of individual subject and group change was performed utilizing a two-tailed *t* test. Findings: No structural imaging change was noted on T2-weighted or three-dimensional fluid-attenuated inversion recovery imaging between MRI 1 and MRI 2. No absolute difference in dynamic contrast perfusion was observed. A trend ($p = 0.084$) toward increase in interstitial extra-axonal fluid was noted. When individual subjects were examined, this trend toward increased extra-axonal fluid paralleled a decrease in contrast perfusion rate. Discussion/Impact/Recommendations: This study demonstrates high reproducibility of quantitative noninvasive MRI, suggesting MRI is an appropriate assessment tool for TBI and hypobaric-induced injury research in swine. The lack of fluid-attenuated inversion recovery change may be multifactorial and requires further investigation. A trend toward increased extra-axonal water content that negatively correlates with dynamic contrast perfusion implies generalized axonal injury was induced. This study suggests this is a potential model for hypobaric-induced injury as well as potentially other axonal injuries such as TBI in which similar subcortical white matter change occurs. Further development of this model is necessary.

15. SUBJECT TERMS
Hypobaria, swine, MRI

16. SECURITY CLASSIFICATION OF:			17. LIMITATION OF ABSTRACT	18. NUMBER OF PAGES	19a. NAME OF RESPONSIBLE PERSON
a. REPORT	b. ABSTRACT	c. THIS PAGE			Dr. Stephen McGuire
U	U	U	SAR	10	19b. TELEPHONE NUMBER *(include area code)*

Utilization of MRI for Cerebral White Matter Injury in a Hypobaric Swine Model—Validation of Technique

Jennifer A. McGuire, AS†; Col Paul M. Sherman, USAF MC‡§; Erica Dean, BSN‡; Maj Jeremy M. Bernot, USAF MC§; Laura M. Rowland, PhD*; Col Stephen A. McGuire, USAF MC (Ret.)‡¶; Peter V. Kochunov, PhD**

ABSTRACT Background: Repetitive hypobaric exposure in humans induces subcortical white matter change, observable on magnetic resonance imaging (MRI) and associated with cognitive impairment. Similar findings occur in traumatic brain injury (TBI). We are developing a swine MRI-driven model to understand the pathophysiology and to develop treatment interventions. Methods: Five miniature pigs (*Sus scrofa domestica*) were repetitively exposed to nonhypoxic hypobaria (30,000 feet/FIO_2 100%/transcutaneous PO_2 >90%) while under general anesthesia. Three pigs served as controls. Pre-exposure and postexposure MRIs were obtained that included structural sequences, dynamic contrast perfusion, and diffusion tensor quantification. Statistical comparison of individual subject and group change was performed utilizing a two-tailed *t* test. Findings: No structural imaging change was noted on T2-weighted or three-dimensional fluid-attenuated inversion recovery imaging between MRI 1 and MRI 2. No absolute difference in dynamic contrast perfusion was observed. A trend ($p = 0.084$) toward increase in interstitial extra-axonal fluid was noted. When individual subjects were examined, this trend toward increased extra-axonal fluid paralleled a decrease in contrast perfusion rate. Discussion/Impact/Recommendations: This study demonstrates high reproducibility of quantitative noninvasive MRI, suggesting MRI is an appropriate assessment tool for TBI and hypobaric-induced injury research in swine. The lack of fluid-attenuated inversion recovery change may be multifactorial and requires further investigation. A trend toward increased extra-axonal water content that negatively correlates with dynamic contrast perfusion implies generalized axonal injury was induced. This study suggests this is a potential model for hypobaric-induced injury as well as potentially other axonal injuries such as TBI in which similar subcortical white matter change occurs. Further development of this model is necessary.

INTRODUCTION

Increased subcortical white matter hyperintensity (WMH) burden on magnetic resonance imaging (MRI) is associated with nonhypoxic hypobaric occupational exposure in U-2 pilots and in altitude chamber inside safety monitors.[1–3] Additionally, divers have increased WMH burden.[4] Extreme mountain climbers have white matter (WM) volume change[5] and diffusion tensor imaging (DTI) changes[6,7] and U-2 pilots have DTI change after excluding contribution from WMH.[8] Recently, we have demonstrated that a single hypobaric exposure in humans does not induce acute WM hyperintensities on fluid-attenuated inversion recovery (FLAIR) but is associated with other transient MRI changes (P. Sherman, S. McGuire, personal communication; August 2, 2016). All of these populations experience decompressive stress and are at risk of decompression sickness. Reduced executive cognitive performance has been linked to WMH burden[9,10] and disruption of axonal integrity as measured by DTI.[11,12] The traditional neuropathological model posits gaseous embolic damage to the brain as the main mechanism responsible for hypobaric-induced brain injury, although the possibilities of microemboli and/or inflammatory and/or immunological etiologies inciting a more diffuse process have been suggested.[13–16] Given the presumed permanence of the subcortical WM brain injury and reduced neurocognitive performance associated with hypobaric exposure, an animal model is necessary to understand the pathophysiology and to develop prevention and treatment interventions.

We are developing a translational neuroimaging animal model to understand the physiology of diffuse brain injury following nonhypoxic hypobaric exposure. We chose the miniature pig (*Sus scrofa domestica*) as the animal model because of the close resemblance of the pig gyrencephalic brain to the human brain in both white-to-grey matter ratio and in cerebral circulation. Likewise, the same MRI scanner and sequences can be used in both humans and miniature pigs, providing a translational component to this research. Although large animals with a greater degree of WM would have been ideal, the size of the hypobaric chamber and the

*Conte Center, Maryland Psychiatric Research Center, University of Maryland School of Medicine, 55 Wade Avenue, Catonsville, MD 21228.

†Oxford College of Emory University, 810 Whatcoat Street, Oxford, GA 30054.

‡U.S. Air Force School of Aerospace Medicine, Aeromedical Research Department, 2510 5th Street, Building 840, Wright-Patterson AFB, OH 45433-7913.

§Department of Neuroradiology, 59th Medical Wing, 2200 Bergquist Drive, Suite 1, Room 7A45, Joint Base San Antonio-Lackland AFB, TX 78236.

‖Clinical Research Department, 59th Medical Wing, 2200 Bergquist Drive, Suite 1, Joint Base San Antonio-Lackland AFB, TX 78236.

¶Department of Neurology, 59th Medical Wing, 2200 Bergquist Drive, Suite 1, Joint Base San Antonio-Lackland AFB, TX 78236.

The views expressed in this article are those of the authors and do not necessarily reflect the official policy or position of the Air Force, the Department of Defense, or the U.S. Government.

doi: 10.7205/MILMED-D-16-00188

desire to employ the same MRI sequences utilized in our human studies[3] restricted the animal model to a weight of 20 to 25 kg.

We hypothesized that the MRI changes in this model would parallel the changes reported in humans. We studied diffusion changes in cerebral WM using the T2-weighted three-dimensional (3-D) FLAIR, dynamic susceptibility contrast (DSC), and advanced diffusion-weighted signal with a longitudinal imaging approach. DSC utilizes a contrast agent to assess vascular integrity. Advanced diffusion-weighted signal (multi-*b*-value and permeability–diffusivity [PD]) assesses a two-compartment restricted and unrestricted water model to assess changes in interstitial water content. As the hypobaric injuries in humans are mainly observed in the cerebral WM, the amount of WM in the brain of the miniature pig compared to rodent models would increase the likelihood of finding WMH on MRI and neuropathological examination.

METHODS

Animal Subjects

All animal protocols were reviewed and approved by the Institutional Animal Care and Use Committee, 59th Medical Wing, Joint Base San Antonio-Lackland AFB, Texas. Seventeen miniature female pigs (14 study subjects; 3 control subjects) weighing 19 to 24 kg were used. Six subject animals were lost to severe pulmonary injury from ventilator barotrauma and/or severe pulmonary decompression sickness with subsequent overwhelming sepsis before MRI 2, and two sustained cardiac arrest during altitude exposure and one experienced a fatal anaphylactic allergic reaction to propofol, leaving eight animals available for baseline and postexposure MRI assessment (five subjects and three controls; Table I). Only female pigs were used, as bladder catheterization was necessary for fluid monitoring during the prolonged periods of anesthesia for the chamber exposures and for the MRIs. All animals underwent the same procedures, including placement in the barometric chamber for 8 hours while under general anesthesia, the only difference being hypobaric exposure. The three control animals were maintained at sea level on room air in the chamber, whereas the subject animals were taken to 9,144 m (30,000 feet) on 100% oxygen. All imaging was performed at the Wilford Hall Ambulatory Surgical Center, 59th Medical Wing. Animals were housed in the center's animal facilities.

Study Protocol

Anesthesia during imaging was maintained using isoflurane via an MRI-compatible anesthesia machine. Since gaseous anesthesia was unreliable at altitude, anesthesia during active/sham hypobaric exposure was maintained using periodic boluses of propofol/ketamine adjusted to maintain stable physiological parameters and anesthesia. On study day 1, baseline imaging was performed. Exposure episodes began on study day 3 with three subject animals exposed six times to 9,144 meters (ascent/descent time 15 minutes) over 12 days, one exposed five times and one exposed four times. Three control animals underwent six sham exposures at sea level. Following intubation, all animals received 1 hour of 100% oxygen prebreathe before active or sham exposure. Animals taken to altitude remained on 100% oxygen and the sham animals were placed on room air at sea level. As ventilator adjustments were not possible once a subject animal was in the chamber, tidal volumes were preset on the basis of weight and volume calculations derived from Boyle's law. Throughout exposure, transcutaneous pulse oxygen >90 mmHg and endotracheal tube carbon dioxide 35 to 45 mmHg were maintained by drug infusion adjustment. Chamber temperature was maintained between 68 and 70°F. Fluid input was adjusted to match urine output. On study day 15 (2 days after final exposure), a second MRI was performed. Subsequently, all animals were euthanized with sodium pentobarbital. Necropsy including neuropathological examination of neural tissue was performed.

Magnetic Resonance Imaging

All imaging data were collected at the Wilford Hall Ambulatory Surgical Center, 59th Medical Wing, Joint Base San Antonio-Lackland, Texas, using a Siemens 3T Verio scanner (Siemens Medical Solutions USA, Inc., Malvern, Pennsylvania) equipped with a 15-channel phased array knee coil applied as a head coil for pigs in the prone position. The protocol consisted of high-resolution T2-weighted FLAIR sequence, multi-*b*-value diffusion-weighted imaging protocol, and DSC.

TABLE I. Subject Specifics

Subject	Weight/Sex (kg/F)	Flights	Cause of Death
Control 1	19	6	Euthanized after MRI 2
Control 2	19	6	Euthanized after MRI 2
Control 3	22.5	6	Euthanized after MRI 2
Subject 1	17	6	Barotrauma-induced death 3 days after MRI 2
Subject 2	20	4	Euthanized after MRI 3
Subject 3	22	5	Euthanized after MRI 3
Subject 4	24	6	Euthanized after MRI 3
Subject 5	19	6	Fatal sepsis resulting from severe sinusitis 6 days after MRI 2

T2-Weighted FLAIR Imaging and Analysis

Three-dimensional FLAIR provides structural imaging of the brain with the suppression of cerebrospinal fluid signal.[17] Imaging was performed in a similar manner to previously reported human studies[3] except with an isotropic resolution of 0.30 × 0.30 × 0.30 mm. A 3-D turbo spin-echo sequence used the following parameters: TR = 4,500 milliseconds, TE = 311 milliseconds, flip angles = 90/180, echo train length of 224, and nonselective inversion pulse with TI = 1,800 milliseconds.[3] Mango software (http://ric.uthscsa.edu/mango) was used to display the FLAIR images, permitting semiautomatic delineation of WMH lesions by an experienced neuroanatomist as previously described.[2]

Multi-b-Value Imaging Protocol and PD Model Calculations

This protocol was developed on the basis of q-space in vivo mapping of water diffusion.[18–22] This protocol consisted of 15 shells of *b* values (*b* = 250, 500, 600, 700, 800, 900, 1,000, 1,250, 1,500, 1,750, 2,000, 2,500, 3,000, 3,500, and 3,800 s/mm^2; diffusion gradient duration = 47 milliseconds, separation= 54 milliseconds). Thirty-five isotropically distributed diffusion-weighted directions were collected per shell, including 16 *b* = 0 images. The highest *b* value (*b* = 3,800 s/mm^2) was chosen because the signal-to-noise ratio (SNR) for the corpus callosum (SNR = 6.1 ± 0.7) during protocol development met the empirical requirement of SNR = 5.0. The *b* values and the number of directions per shell were chosen for improved fit of the biexponential model.[23] The data were collected using a single-shot, echo-planar, single refocusing spin-echo, T2-weighted sequence (TE/TR = 120/1,500 millisecond with the FOV = 100 mm) with a spatial resolution of 1 × 1 × 3 mm and 12 slices prescribed in axial orientation to sample the entire brain. The scan time was about 10 minutes.

The WM mask was derived per subject on the basis of the contrast in fractional anisotropy (FA) between WM, GM, and CSF. Voxel-wise FA, D_A, and D_R images were created using Camino software (http://cmic.cs.ucl.ac.uk/camino).[24] Segmentation was semiautomatic for each animal, using an intensity histogram approach and manual editing in the Mango software.

The PD model was presented elsewhere,[25] using parameters derived from the following biexponential two-compartment diffusion model fit:

Here S(*b*) is the average diffusion-weighted signal for a given *b* value, averaged across all directions. This model is focused on calculation of M_u, which is the compartmental fraction of the signal that comes from interstitial (unrestricted) water, and $(1 - M_u)$ is the fraction of the compartment with restricted diffusion (M_r). This model assumes that the diffusion signal is produced by two quasi-pools of anisotropically diffusing water. D_u is the mean unrestricted diffusivity of the water molecules that are away from the axonal membranes. D_r is the mean restricted diffusivity of the water molecules that are within the restricted ion channels or close to axonal membranes. The parameters are the compartmental fraction M_u and the PD index (PDI), which is the ratio of D_r and D_u. An increase in M_u would correspond to the rise in the fraction of interstitial water within WM voxels that can be interpreted as unrestricted water molecules that are away from the axonal membrane.

DSC Perfusion Imaging and Analysis

DSC perfusion imaging is a sensitive approach for the evaluation of embolic cerebral damage and change in permeability of the blood brain barrier (BBB).[26,27] DSC utilizes an exogenous contrast imaging agent that historically has been used to study changes in cerebral perfusion and disruptions of the BBB caused by trauma, ischemia, cerebral inflammation, multiple sclerosis, neoplasms, and other conditions.[28,29] Under a normal physiological state, contrast agents used with DSC, such as diethylenetriamine pentaacetic acid bismethylamide chelate of gadolinium (Gd-DTPA; Magnevist; molecular weight 573.3 Da) (Berlex Laboratories, Wayne, New Jersey), cannot cross the BBB. If the BBB is disrupted, the contrast agent enters surrounding tissues and becomes temporarily entrapped in the cellular matrix. This entrapment is detected by alterations in the washout rate and reduced intensity in the affected tissues; specifically, on a susceptibility (T2*) sensitive imaging sequence, Gd-DTPA alters the magnetic relaxation properties of the blood and therefore elongates washout curves, preventing full recovery of imaging intensity.[30] The signal intensity is reduced in linear proportion to the concentration of the contrast agent and, therefore, produces regional reductions in signal proportional to the perfusion rates.

A 10-mL bolus (46.901 mg/mL; mean 23.3 mg Gd-DTPA/kg of body weight; range 19.5–27.6 mg) of Gd-DTPA was administered to the pig through a port-a-catheter inserted 1 week before experiment. The baseline and postexposure imaging protocols included a single DSC study utilizing a gradient echo-planar-imaging perfusion sequence. Parameters were adjusted to obtain high temporal (TR = 2) and spatial (1.6 × 1.6 × 2.0 mm) resolution, acquiring 23 slices for full brain coverage with no gaps. Imaging slices were prescribed axially.

Image preprocessing was performed using Functional Magnetic Resonance Imaging Brain Software Library (http://fsl.fmrib.ox.ac.uk/fsl/fslwiki/) and consisted of motion correction and automated removal of nonbrain tissue. Following this, the average image was loaded in Mango software where the remaining nonbrain tissue was removed via manual detailing.

Mango was used to calculate the average brain intensity measurements for each of the time points of DSC sequence. Value normalization was performed by averaging all intensities before injection (mean data points averaged 64, range

51–65) to produce an average baseline. The measured intensities were then normalized using the equation:

$$Normalized = \frac{Measured\ Intensity - Min\ Intensity}{Avg\ Initial\ \ Baseline - \ \ Min\ Intensity}$$

where "Normalized Intensity" is the value corresponding to the normalized 0-1 scale, "Measured Intensity" is the original intensity value, "Avg Initial Baseline" is the average of the first 51 to 65 points before injection of the Gd-DTPA, and "Min Intensity" is the minimum intensity following the injection of Gd-DTPA. Normalized signal intensity trends were shifted to have the minimum value at time point 72 (140 seconds) to accommodate for potential variability in the time of injection.

The recovery of signal intensity corresponding to the washout of contrast agent from the brain was fit using a natural logarithmic function: Intensity = A × ln(t) + B, where t is the time and A and B are fit constants. For this equation, t = 0 corresponds to the minimum intensity at point 72 (140 seconds). The washout rate was derived from the average of the first derivative values of the functional model for the initial washout, using the equation:

$$\frac{dI}{dt} = \frac{A}{t}$$

where dI/dt is the first derivative, A is the fit constant from the original equation, and t is time. The postcontrast intensity was the average of the final function values. The washout rate and final value were used to evaluate changes between the first and second imaging of each subject. The intensities for the sham and active animals were averaged respectively, and the same procedure was applied.

Statistical Analysis

Individual subject baseline and postexposure results were compared using 2-tailed paired t tests to evaluate changes between the first and second imaging of each subject. Additionally, a 2-tailed normal t test was used for group comparison of sham and active subject results. We used chi-squared and Spearman's correlation factor for assessment of validity of observed versus derived equation equivalency. We considered $p < 0.05$ to be significant.

RESULTS

There was no group difference in the body weight between sham and active animals (p = 0.89). No WMH lesions or vasogenic edema changes were detected on the baseline or follow-up T2-weighted or 3-D FLAIR images (Fig. 1).

There were no significant changes in the M_u in sham or PDI coefficients in active and sham animals, although there was a trend toward an increase in M_u between the baseline and follow-up in active subjects (Table II; p = 0.084).

A tight fit of the observed averaged DSC data to the exponential function was present (Fig. 2). There were no significant differences in the fit parameters between baseline and follow-up imaging sessions in both sham and active animals (Table III). Likewise, there were no significant differences between baseline and follow-up measurements of the washout rate and the ratio of final/baseline intensity parameters for the sham or active animals (Table III). Finally, comparing the washout rate and the ratio final/baseline intensity for sham to active animals, no significant differences were found between the baseline and follow-up imaging between groups (all $p > 0.05$).

Correlation of DSC to M_u suggested an inverse relationship between washout rate and M_u, with increased unrestricted interstitial water associated with decreased Gd-DTPA elimination

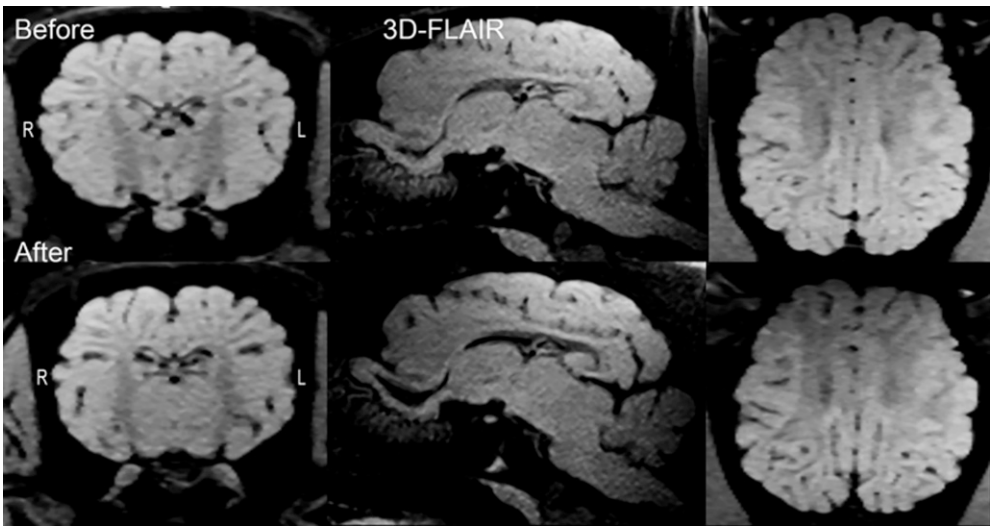

FIGURE 1. Pre- and postexposure 3-D FLAIR image. Coronal, sagittal, and axial representative images demonstrate clear separation of white and gray matter. No WM hyperintense lesions were apparent in the subcortical and periventricular regions.

TABLE II. PD-Model Analysis of Diffusion-Weighted Data

	MRI 1 (Pre-exposure)		MRI 2 (Postexposure)		*p* Value Pre/Post	
Item	M_u	PDI	M_u	PDI	M_u	PDI
Sham Average	0.5874	0.0898	0.5937	0.0935	0.128	0.136
SD	0.0047	0.0013	0.0015	0.0011		
CI	0.0053	0.0014	0.0017	0.0012		
Study Average	0.5897	0.0865	0.5985	0.1076	0.084	0.378
SD	0.0054	0.0083	0.0102	0.0460		
CI	0.0048	0.0073	0.0090	0.0403		

CI, 95% confidence interval; SD, standard deviation.

(sham animals: $y = -51.538x + 56.699$; $R^2 = 0.8979$; study subjects $y = -2.7973x + 5.4942$; $R^2 = 0.0194$).

Neuropathological examination demonstrated neuropil clear spaces, gliotic changes, subarachnoid and WM microhemorrhages, thoracic spinal cord perivascular microhemorrhage, arachnoidal inflammation, focal red Purkinje cells, focal collection of oligodendrocytes, and focal bacterial inflammation.

DISCUSSION

Our study demonstrated an excellent stability of the quantitative MRI measurements in both active and sham animals and the feasibility of this approach in a miniature pig model of hypobaric brain injury. The hypobaric exposure demonstrated no observable WMH changes in the active animals. WMH are nonspecific[31–35] but have been associated in two human populations exposed to hypobaria after controlling for other potential etiologies.[3] The failure to demonstrate formation of WMH in this study may be secondary to insufficient exposure stimulus, to lack of sufficient follow-up for WMH development, or to inherent resistance of miniature swine to developing cerebral WMH lesions. The small size of this study further limits the demonstration of significance; human studies on hypobaric-associated WMH examined 83 to 106 subjects per group.[3] Postmortem examination in this study noted a number of nonspecific changes, but how these potentially relate to WMH or directly to hypobaric exposure is unclear. Pathological correlation to WMH in humans has occurred[36] but to our knowledge this has not occurred in swine.

No statistically different changes were noted in DSC. A trend was noted in the fraction of unrestricted interstitial (extra-axonal) water (M_u) on the analysis of the diffusion-weighted images. Furthermore, there was an inverse correlation of M_u with Gd-DTPA washout, suggesting injury had possibly occurred in active subjects as manifested by increased interstitial extra-axonal water and delayed clearance of Gd-DTPA. These results would be consistent with a decrease in diffusivity with histopathological evidence of axonal injury in rats following traumatic brain injury.[37,38]

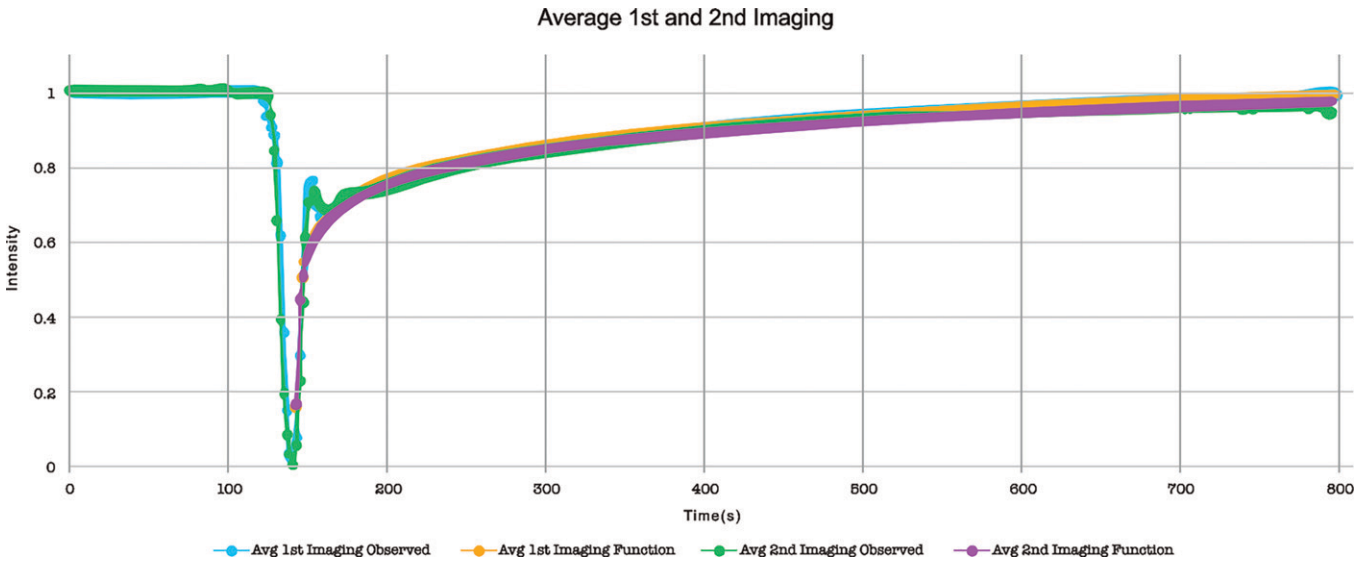

FIGURE 2. Comparison of actual observed group data to exponential function for both the first and second MRIs. On both occasions, the actual data tightly follow the derived exponential function (χ^2, $p = 0.2395$; Spearman's correlation, $p <$ e-16), permitting cross group comparison of the regression equation parameters.

TABLE III. Nonlinear Regression Equation Parameters and Washout Rate and Ratio

	MRI 1 (Pre-exposure)		MRI 2 (Postexposure)		t Value/*p* Value	
Group	A	B	A	B	A	B
Sham	0.087 ± 0.002	0.439 ± 0.030	0.085 ± 0.016	0.435 ± 0.078	0.217/0.86	0.095/0.91
Study	0.100 ± 0.014	0.342 ± 0.113	0.098 ± 0.008	0.336 ± 0.056	0.269/0.80	0.107/0.93
	Washout Rate	Intensity Ratio	Washout Rate	Intensity Ratio	Washout Rate	Intensity Ratio
Sham	0.262 ± 0.048	0.995 ± 0.041	0.265 ± 0.090	0.975 ± 0.032	−0.047/0.97	0.679/0.68
Study	0.262 ± 0.048	0.262 ± 0.048	0.262 ± 0.048	0.262 ± 0.048	0.180/0.79	0.895/0.34

A and B are fit coefficients from Intensity = A × ln(t) + B where t = time. Intensity ratio = final/base intensity.

Repeated anesthesia and MRI in the sham animals did not produce any significant changes on these indices sensitive to WM integrity. This suggests the observed MRI changes were possibly related to the hypobaric exposure, although other contributing factors cannot be excluded.

The lack of new WMH lesions in this model is consistent with similar findings of an in-progress single exposure human study. We posit that the initial injury is a diffuse process and that subsequent FLAIR change occurs in those instances where repair has been inadequate. With this hypothesis, initial injury might be reflected by BBB integrity and interstitial fluid content changes, although FLAIR change would not be expected. Although the M_u trend data and its relationship to Gd-DTPA washout rate are encouraging, the lack of significant difference in other parameters suggests this pig model of cerebral injury from hypobaria needs further development.

One substantial difference between this model and occupational hypobaric exposure in humans is that the animals were exposed while under anesthesia. Humans are awake and active during occupational exposure, and physical activity at altitude is known to potentiate brain injury.[39] In addition, anesthesia may act as a neuroprotective agent, thus making the animal experiments less realistic. Necropsy suggested the high mortality rate in this study was secondary to the combination of decompression sickness and/or ventilator-associated barotrauma with severe pulmonary injury and sepsis. Although neuropathological abnormalities were observed, the relationship to possible hypobaric-induced injury is unclear. These issues are being addressed by utilizing a nonanesthetized, physically active pig in a phase II trial. Additionally, this phase II model utilizes an expanded set of quantitative structural (T1 and T2 weighted) and physiological (microstructural properties of molecular diffusion, DSC, and concentrations of neurochemicals) parameters for a more comprehensive assessment of the pathophysiological process.

The consistency of measurements in this model suggests that MRI can be used in a miniature swine model to study brain trauma induced not only by hypobaric exposure but resulting from other factors. Susceptibility-weighted perfusion MRI may be difficult to obtain in the acute TBI setting secondary to patient contraindications and is limited by signal loss in the presence of blood products, but may be valuable in subacute or chronic TBI particularly when combined with other conventional and advanced MRI techniques including DTI.[40–42] Patients with mild TBI and normal conventional imaging have demonstrated perfusion deficits that correlate with neurocognitive impairment.[43,44] TBI causes axonal and capillary disruption[45] that can be observed as WMH on FLAIR MRI.[44,46–48] DTI can detect microscopic tissue damage in TBI and other central nervous system disorders, particularly those that affect WM, and provide markers that may be capable of predicting clinical outcome.[40,41,43,44] Thus, although the focus of this study has been on brain injury following hypobaric exposure, the findings from this model are likely to be relevant for mild-to-moderate TBI, thus avoiding the focal cerebral injury associated with other animal models. This model suggests a general disruption of axons has occurred, possibly similar to the shear injury in TBI. Thus, potentially this model might provide insight into the injury biomechanics and axonal pathophysiology of TBI, hence addressing one of the major contributors to subsequent disability.

ACKNOWLEDGMENTS

The authors wish to thank Elaine "Sandy" Kawano, U.S. Air Force School of Aerospace Medicine, 711th Human Performance Wing, Wright-Patterson AFB, Ohio, for scientific editorial assistance, and they also acknowledge radiology, neurology, and pathology resident participation in swine research project. This research was supported by P50MH103222 (Conte Summer Undergraduate Research Program to J.A.M.), a U.S. Air Force Surgeon General grant (711HPW FA8650-10-D-6052 0048) and 59th Medical Wing, Clinical Research Division, Graduate Medical Education grant to P.M.S., and a National Institute of Biomedical Imaging and Bioengineering grant (R01EB015611) to P.V.K.

REFERENCES

1. McGuire S, Sherman P, Profenna L, et al: White matter hyperintensities on MRI in high-altitude U-2 pilots. Neurology 2013; 81(8): 729–35.
2. McGuire SA, Sherman PM, Brown AC, et al: Hyperintense white matter lesions in 50 high-altitude pilots with neurologic decompression sickness. Aviat Space Environ Med 2012; 83(12): 1117–22.

3. McGuire SA, Sherman PM, Wijtenburg SA, et al: White matter hyperintensities and hypobaric exposure. Ann Neurol 2014; 76(5): 719–26.
4. Zhang H, Lin J, Sun Y, et al: Compromised white matter microstructural integrity after mountain climbing: evidence from diffusion tensor imaging. High Alt Med Biol 2012; 13(2): 118–25.
5. Connolly DM, Lee VM: Odds ratio meta-analysis and increased prevalence of white matter injury in healthy divers. Aerosp Med Hum Perform 2015; 86(1): 928–35.
6. Kottke R, Hefti J, Rummel C, Hauf M, Hefti U, Merz T: Morphological brain changes after climbing to extreme altitudes—a prospective cohort study. PLoS One 2015; 10(10): e0141097.
7. Wong SH, Turner N, Birchall D, Walls TJ, English P, Schmid ML: Reversible abnormalities of DWI in high-altitude cerebral edema. Neurology 2004; 62(2): 335–6.
8. McGuire SA, Boone GRE, Sherman PM, et al: White matter integrity in high-altitude pilots exposed to hypobaria. Aerosp Med Hum Perform 2016; 87(12): 983–8.
9. McGuire SA, Tate DF, Wood J, et al: Lower neurocognitive function in U-2 pilots: relationship to white matter hyperintensities. Neurology 2014; 83(7): 638–45.
10. Kloppenborg RP, Nederkoorn PJ, Geerlings MI, van den Berg E: Presence and progression of white matter hyperintensities and cognition: a meta-analysis. Neurology 2014; 82(23): 2127–38.
11. Nowrangi MA, Okonkwo O, Lyketsos C, et al: Atlas-based diffusion tensor imaging correlates of executive function. J Alzheimers Dis 2015; 44(2): 585–98.
12. Lawrence AJ, Chung AW, Morris RG, Markus HS, Barrick TR: Structural network efficiency is associated with cognitive impairment in small-vessel disease. Neurology 2014; 83(4): 304–11.
13. Balldin UI, Pilmanis AA, Webb JT: Central nervous system decompression sickness and venous gas emboli in hypobaric conditions. Aviat Space Environ Med 2004; 75(11): 969–72.
14. Vann RD, Butler FK, Mitchell SJ, Moon RE: Decompression illness. Lancet 2011; 377(9760): 153–64.
15. Foster PP, Butler BD: Decompression to altitude: assumptions, experimental evidence, and future directions. J Appl Physiol (1985) 2009; 106(2): 678–90.
16. Thom SR, Yang M, Bhopale VM, Huang S, Milovanova TN: Microparticles initiate decompression-induced neutrophil activation and subsequent vascular injuries. J Appl Physiol (1985) 2011; 110(2): 340–51.
17. Gilman S: Imaging the brain. First of two parts. N Engl J Med 1998; 338(12): 812–20.
18. Sukstanskii AL, Ackerman JJ, Yablonskiy DA: Effects of barrier-induced nuclear spin magnetization inhomogeneities on diffusion-attenuated MR signal. Magn Reson Med 2003; 50(4): 735–42.
19. Sukstanskii AL, Yablonskiy DA, Ackerman JJ: Effects of permeable boundaries on the diffusion-attenuated MR signal: insights from a one-dimensional model. J Magn Reson 2004; 170(1): 56–66.
20. Yablonskiy DA, Sukstanskii AL: Theoretical models of the diffusion weighted MR signal. NMR Biomed 2010; 23(7): 661–81.
21. Wu YC, Field AS, Whalen PJ, Alexander AL: Age- and gender-related changes in the normal human brain using hybrid diffusion imaging (HYDI). Neuroimage 2011; 54(3): 1840–53.
22. Clark CA, Hedehus M, Moseley ME: In vivo mapping of the fast and slow diffusion tensors in human brain. Magn Reson Med 2002; 47(4): 623–8.
23. Jones DK, Horsfield MA, Simmons A: Optimal strategies for measuring diffusion in anisotropic systems by magnetic resonance imaging. Magn Reson Med 1999; 42(3): 515–25.
24. Alexander DC, Hubbard PL, Hall MG, et al: Orientationally invariant indices of axon diameter and density from diffusion MRI. Neuroimage 2011; 52(4): 1374–89.
25. Kochunov P, Chiappelli J, Hong LE: Permeability-diffusivity modeling vs. fractional anisotropy on white matter integrity assessment and application in schizophrenia. Neuroimage Clin 2013; 3: 18–26.
26. Kluytmans M, van der Grond J, Viergever MA: Gray matter and white matter perfusion imaging in patients with severe carotid artery lesions. Radiology 1998; 209(3): 675–82.
27. Nasel C, Azizi A, Veintimilla A, Mallek R, Schindler E: A standardized method of generating time-to-peak perfusion maps in dynamic-susceptibility contrast-enhanced MR imaging. AJNR Am J Neuroradiol 2000; 21(7): 1195–8.
28. Hamberg LM, Macfarlane R, Tasdemiroglu E, et al: Measurement of cerebrovascular changes in cats after ischemia using dynamic magnetic resonance imaging. Stroke 1993; 24(3): 444–50.
29. Kochunov P, Castro C, Davis DM, et al: Fetal brain during a binge drinking episode: a dynamic susceptibility contrast MRI fetal brain perfusion study. Neuroreport 2010; 21(10): 716–21.
30. Navarathna DH, Munasinghe J, Lizak MJ, Nayak D, McGavern DB, Roberts DD: MRI confirms loss of blood-brain barrier integrity in a mouse model of disseminated candidiasis. NMR Biomed 2013; 26(9): 1125–34.
31. Kochunov P, Thompson PM, Coyle TR, et al: Relationship among neuroimaging indices of cerebral health during normal aging. Hum Brain Mapp 2008; 29(1): 36–45.
32. Kennedy KM, Raz N: Pattern of normal age-related regional differences in white matter microstructure is modified by vascular risk. Brain Res 2009; 1297: 41–56.
33. Hamedani AG, Rose KM, Peterlin BL, et al: Migraine and white matter hyperintensities: the ARIC MRI study. Neurology 2013; 81(15): 1308–13.
34. Kim H, Yun CH, Thomas RJ, et al: Obstructive sleep apnea as a risk factor for cerebral white matter change in a middle-aged and older general population. Sleep 2013; 36(5): 709–15.
35. Bigler ED, Abildskov TJ, Petrie J, et al: Heterogeneity of brain lesions in pediatric traumatic brain injury. Neuropsychology 2013; 27(4): 438–51.
36. Fazekas F, Kleinert R, Offenbacher H, et al: Pathologic correlates of incidental MRI white matter signal hyperintensities. Neurology 1993; 43(9): 1683–9.
37. Mac Donald CL, Dikranian K, Song SK, Bayly PV, Holtzman DM, Brody DL: Detection of traumatic axonal injury with diffusion tensor imaging in a mouse model of traumatic brain injury. Exp Neurol 2007; 205(1): 116–31.
38. Mac Donald CL, Dikranian K, Bayly P, Holtzman D, Brody D: Diffusion tensor imaging reliably detects experimental traumatic axonal injury and indicates approximate time of injury. J Neurosci 2007; 27(44): 11869–76.
39. Webb JT, Beckstrand DP, Pilmanis AA, Balldin UI: Decompression sickness during simulated extravehicular activity: ambulation vs. non-ambulation. Aviat Space Environ Med 2005; 76(8): 778–81.
40. Wintermark M, Sanelli PC, Anzai Y, Tsiouris AJ, Whitlow CT, American College of Radiology Head Injury Institute: Imaging evidence and recommendations for traumatic brain injury: advanced neuro- and neurovascular imaging techniques. AJNR Am J Neuroradiol 2015; 36(2): E1–11.
41. Hulkower MB, Poliak DB, Rosenbaum SB, Zimmerman ME, Lipton ML: A decade of DTI in traumatic brain injury: 10 years and 100 articles later. AJNR Am J Neuroradiol 2013; 34(11): 2064–74.
42. Wu X, Kirov II, Gonen O, Ge Y, Grossman RI, Lui YW: MR imaging applications in mild traumatic brain injury: an imaging update. Radiology 2016; 279(3): 693–707.
43. Grossman EJ, Jensen JH, Babb JS, et al: Cognitive impairment in mild traumatic brain injury: a longitudinal diffusional kurtosis and perfusion imaging study. AJNR Am J Neuroradiol 2013; 34(5): 951–7.
44. Fakhran S, Yaeger K, Alhilali L: Symptomatic white matter changes in mild traumatic brain injury resemble pathologic features of early Alzheimer dementia. Radiology 2013; 269(1): 249–57.
45. Smith DH, Meaney DF, Shull WH: Diffuse axonal injury in head trauma. J Head Trauma Rehabil 2003; 18(4): 307–16.

46. Mac Donald CL, Johnson AM, Cooper D, et al: Detection of blast-related traumatic brain injury in U.S. military personnel. N Engl J Med 2011; 364(22): 2091–2100.
47. Moen KG, Skandsen T, Folvik M, et al: A longitudinal MRI study of traumatic axonal injury in patients with moderate and severe traumatic brain injury. J Neurol Neurosurg Psychiatry 2012; 83(12): 1193–200.
48. Hou DJ, Tong KA, Ashwal S, et al: Diffusion-weighted magnetic resonance imaging improves outcome prediction in adult traumatic brain injury. J Neurotrauma 2007; 24(10): 1558–69.